RAA 2019 Vol. **19** No. **5**, 64(14pp) doi: 10.1088/1674–4527/19/5/64

http://www.raa-journal.org *http://iopscience.iop.org/raa*

Research in Astronomy and Astrophysics

EDITOR'S RECOMMENDATION

More than two hundred and fifty thousand spectroscopic binary or variable star candidates discovered by LAMOST

Sheng-Bang Qian[1,2,3,4], Xiang-Dong Shi[1,2,3,4], Li-Ying Zhu[1,2,3,4], Lin-Jia Li[1,2,3], Jia Zhang[1,2,3], Er-Gang Zhao[1,2,3], Zhong-Tao Han[1,2,3], Xiao Zhou[1,2,3], Xiao-Hui Fang[1,2,3,4] and Wen-Ping Liao[1,2,3]

[1] Yunnan Observatories, Chinese Academy of Sciences, Kunming 650216, China; *qsb@ynao.ac.cn*
[2] Key Laboratory of the Structure and Evolution of Celestial Objects, Chinese Academy of Sciences, Kunming 650216, China
[3] Center for Astronomical Mega-Science, Chinese Academy of Sciences, Beijing 100101, China
[4] University of Chinese Academy of Sciences, Beijing 100049, China

Received 2019 February 23; accepted 2019 March 1

Abstract About 786.4 thousand stars were observed by LAMOST twice or more during the first stage of its spectroscopic survey. The radial velocity differences for about 256 thousand targets are larger than $10\,\mathrm{km\,s^{-1}}$ and they are possible spectroscopic binary or variable candidates (SBVCs). It is shown that most SBVCs are slightly metal poorer than the Sun. There are two peaks in the temperature distribution of SBVCs around 5760 K and 4870 K, while there are three peaks in the distribution of the gravitational acceleration at 2.461, 4.171 and $4.621\,\mathrm{cm\,s^{-2}}$. The locations of SBVCs on the [Fe/H]-T, [Fe/H]-$\log g$, $\log g$-T and H-R diagrams are investigated. It is found that the detected SBVCs could be classified into four groups. The first group has higher $\log g \sim 4.621$ and lower $T \sim 4870\,\mathrm{K}$ which are mainly cool red dwarf binaries. The second group of SBVCs has $\log g$ around $4.171\,\mathrm{cm\,s^{-2}}$ that includes binaries and pulsating stars such as δ Sct and γ Dor variables. The gravitational accelerations of the third group of SBVCs are higher and some of them are below the zero-age main sequence. They may be contact binaries in which the primary components are losing energy to the secondaries in the common envelopes and are at a special stellar evolutionary stage. The last group is composed of giants or supergiants with $\log g$ around $2.461\,\mathrm{cm\,s^{-2}}$ that may be evolved pulsating stars. One target (C134624.29+333921.2) is confirmed as an eclipsing binary with a period of 0.65 days. A preliminary analysis suggests that it is a detached binary with a mass ratio of 0.46. The primary fills its critical Roche lobe by about 89%, indicating that mass transfer will occur between the two components.

Key words: stars: fundamental parameters — stars: binaries : spectroscopic — stars: oscillations — stars: binaries : eclipsing — stars: variables: other

1 INTRODUCTION

As both component stars in a spectroscopic binary are orbiting their common center of mass, the orbital velocities will have components in the line of sight and the radial velocities will vary periodically because of the Doppler effect unless the plane of the orbit happens to be perpendicular to the line of sight. By measuring the radial velocities of one or both components, we could detect a binary star. When a binary star happens to orbit in a plane along the line of sight, both components will eclipse and transit each other. These systems are called eclipsing binaries (EBs). EBs are important targets because they enable the most precise ways to determine stellar physical parameters without the use of stellar models (Andersen 1991; Torres et al. 2010, and references therein). Binary stars can be divided into three groups, i.e., detached, semi-detached and contact binary systems, which can be interpreted as different evolutionary stages. The strong interactions between both components are related with many astrophysical processes such as mass transfer and accretion, common envelope evolution and different stellar outbursts. On the other hand, stellar radial velocities could also vary due to a periodical swelling and shrinking of the star or other types of movements such as an expanding gas shell. Pulsating stars or some special giants and supergiants could be found by measuring their radial velocities. They are a good source to study stellar internal structure and stellar evolution.

The Large Sky Area Multi-Object Fiber Spectroscopic Telescope (LAMOST) is a special telescope that is used for low-resolution spectroscopic surveys (Wang et al. 1996; Cui et al. 2012). It has an aperture of about 4 meters with a field of view of about 5 degrees. The spectral wavelength range is from 3700 to 9000 Å and is divided into two arms, i.e., a blue arm (3700–5900 Å) and a red arm (5700–9000 Å). The spectra of about 4000 stars could be obtained by LAMOST in one exposure. Huge amounts of spectroscopic data were obtained by LAMOST (e.g., Zhao et al. 2012, Luo et al. 2015) including pulsating stars (Qian et al. 2018a, 2019) and binary systems (Qian et al. 2017, 2018b). In the time interval between 2011 October 24 and 2017 July 16, more than three million stars were observed by LAMOST. About 786.4 thousand of them were observed twice or more and their stellar atmospheric parameters were obtained. Those data are very useful for detecting new binary and variable candidates.

Based on several photometric surveys around the world, such as the Catalina Sky Survey[1] (CSS, Drake et al. 2009, 2014), the asteroid survey LINEAR[2] (Palaversa et al. 2013), All Sky Automated Survey[3] (ASAS, Pojmanski 1997, Pojmanski et al. 2005) and Northern Sky Variability Survey[4] (NSVS, Woźniak et al. 2004), a large number of variable stars including EBs was discovered. Other wide-field surveys which have contributed to the detections of variable stars are the *Kepler* space telescope (Borucki et al. 2010), *K2* mission (Howell et al. 2014), HATNet survey (Bakos et al. 2004), SuperWASP (Pollacco et al. 2006) and KELT survey (Pepper et al. 2012). Those variables were listed in the International Variable Star Index (VSX)[5], the goal of which is to compile all of that new information together into a single data repository. It provides the tools necessary for controlled and secure revising of the data (e.g., Watson et al. 2006). However, all of these cases are photometric surveys and the spectroscopic properties of those variables are unknown. In the present paper, we present new spectroscopic binary or variable candidates (SBVCs) detected by LAMOST.

[1] `http://www.lpl.arizona.edu/css/`
[2] `https://astroweb.lanl.gov/lineardb/`
[3] `http://www.astrouw.edu.pl/asas/`
[4] `http://www.skydot.lanl.gov/nsvs/nsvs.php`
[5] `http://www.aavso.org/vsx/`

Among the 786.4 thousand stars observed by LAMOST twice or more, about 4575 stars have been listed in VSX. We search for new binary and variable candidates from the other 782 thousand stars. In Section 2, we catalog the stellar atmospheric parameters of about 255.943 thousand stars whose radial velocity differences are larger than $10\,\mathrm{km\,s^{-1}}$ and they are SBVCs. The distributions of those stellar atmospheric parameters for the new SBVCs are presented in Section 3. The multi-color light curves and their associated solutions for the confirmed EB C134624.29+333921.2 (hereafter C1346) are given in Section 4. Several statistical correlations for those new SBVCs are introduced in Section 5. Finally, discussions of the results and conclusions are presented in Section 6.

2 CATALOG OF NEW SBVCS DETECTED BY LAMOST

About 8.17 million stellar spectra with signal to noise (S/N) >10 were obtained during the first stage of the LAMOST spectroscopic survey from 2011 October 24 to 2017 July 16. About 5.34 million of those spectra were used to determine stellar atmospheric parameters when those spectra have higher S/N. Therefore, 5.34 million sets of stellar parameters for about 3.8 million stars were derived including the effective temperature $T_{\rm eff}$, gravitational acceleration $\log(g)$, metallicity [Fe/H] and radial velocity $V_{\rm r}$. They were automatically determined by the LAMOST Stellar Parameter Pipeline (LASP, e.g., Wu et al. 2014; Luo et al. 2015) which is based on the Université de Lyon Spectroscopic Analysis Software (ULySS) (e.g., Koleva et al. 2009, Wu et al. 2011). The standard deviations for $T_{\rm eff}$, $\log g$ and [Fe/H] are 110 K, $0.19\,\mathrm{cm\,s^{-2}}$ and 0.11 dex respectively when $T_{\rm eff} < 8000\,\mathrm{K}$, while that for the radial velocity $V_{\rm r}$ is $4.91\,\mathrm{km\,s^{-1}}$ when $T_{\rm eff} < 10\,000\,\mathrm{K}$ (e.g., Gao et al. 2015). The LAMOST data were compared with other reliable spectral databases, such as high resolution spectral results, SDSS, APOGEE and PASTEL, and were described by Luo et al. (2015). The typical standard deviations from these comparisons are 95 K for T, $0.25\,\mathrm{cm\,s^{-2}}$ for $\log g$, 0.1 dex for [Fe/H] and $7\,\mathrm{km\,s^{-1}}$ for $R_{\rm r}$.

Stellar atmospheric parameters derived by LAMOST were compared by Qian et al. (2018a) with those mainly determined from high-resolution optical spectra from the literature by Frasca et al. (2016). It is shown that there are very good agreements between the two sets of parameters. The standard deviations were derived as 135 K for T, $0.21\,\mathrm{cm\,s^{-2}}$ for $\log g$, 0.14 dex for [Fe/H] and $11\,\mathrm{km\,s^{-1}}$ for $V_{\rm r}$. The LAMOST spectra of about 51 385 stars observed by both the LAMOST and *Kepler* projects were

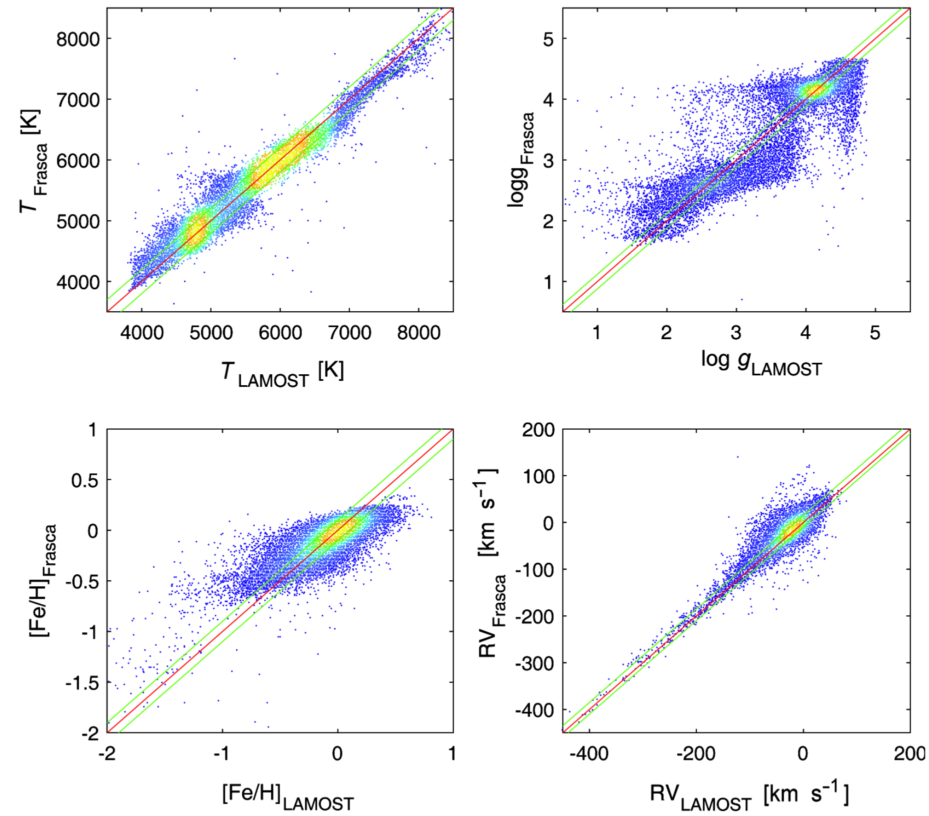

Fig. 1 Comparison between LASP atmospheric parameters of 50 000 stars and those determined with ROTFIT from the LAMOST spectra by Frasca et al. (2016). Also shown as *red lines* in the four panel are the one-to-one relationships. The *green lines* represent a difference of 200 K for T, 0.1 for $\log g$, 0.08 for [Fe/H] and 7 km s^{-1} for $V_{\rm r}$.

analyzed with the code ROTFIT that was developed by Frasca et al. (2003, 2006). Their atmospheric parameters were determined by Frasca et al. (2016). The comparisons between the LAMOST parameters (DR4 and the first three quarters of DR5) and those derived with ROTFIT are displayed in Figure 1 where the red lines in the four panels refer to one-to-one relationships. The green lines represent a difference of 200 K for T, 0.1 cm s^{-2} for $\log g$, 0.08 dex for [Fe/H] and 7 km s^{-1} for $V_{\rm r}$. As shown in the four panels, the yellow parts (which represent most stars) are within the two green lines, indicating that there is good agreement for those parameters obtained by using different codes.

Among the 3.8 million stars, 786.4 thousand of them were observed by LAMOST twice or more. The differences between the lowest and highest radial velocities are calculated. The peak-to-peak radial-velocity amplitude for δ Scuti variables is usually in the range from 5 to 10 km s^{-1} (e.g., Breger et al. 1976; Yang & Walker 1986), while that for γ Dor stars is in the range from 2 to 4 km s^{-1} (e.g., Hatzes 1998; Mathias et al. 2004; De Cat et al. 2006). As mentioned, the standard deviation for radial velocity $V_{\rm r}$ is about 7 km s^{-1}. On the other hand, the changes in radial velocities of some long-period binaries are usually very small because of their small orbital speeds. Therefore, those stars with radial velocity differences larger than 10 km s^{-1} may be SBVCs. After excluding some known variable stars that have been listed in VSX, about 255.943 thousand stars with $\Delta V_{\rm r} > 10$ km s^{-1} are detected that are new SBVCs.

We catalog the stellar atmospheric parameters for those SBVCs. They were observed two or more times and have a radial velocity difference higher than 10 km s^{-1}. For each target, the combined parameter is the weighted mean value of all its observations at different times. The weight for each datum is the inverse square of its error. The final error of the combined parameter is derived with the standard error transfer formula by assuming that each observation is independent of the others. In the catalog, about 1931 stars were observed eight times or more. The distributions of their standard errors along with stellar atmospheric parameters are displayed in the three panels of Figure 2. As shown in the figure, the standard errors for about 90% of those stars are lower than 29 K for T, 0.041 cm s^{-2} for $\log g$ and 0.027 dex for [Fe/H].

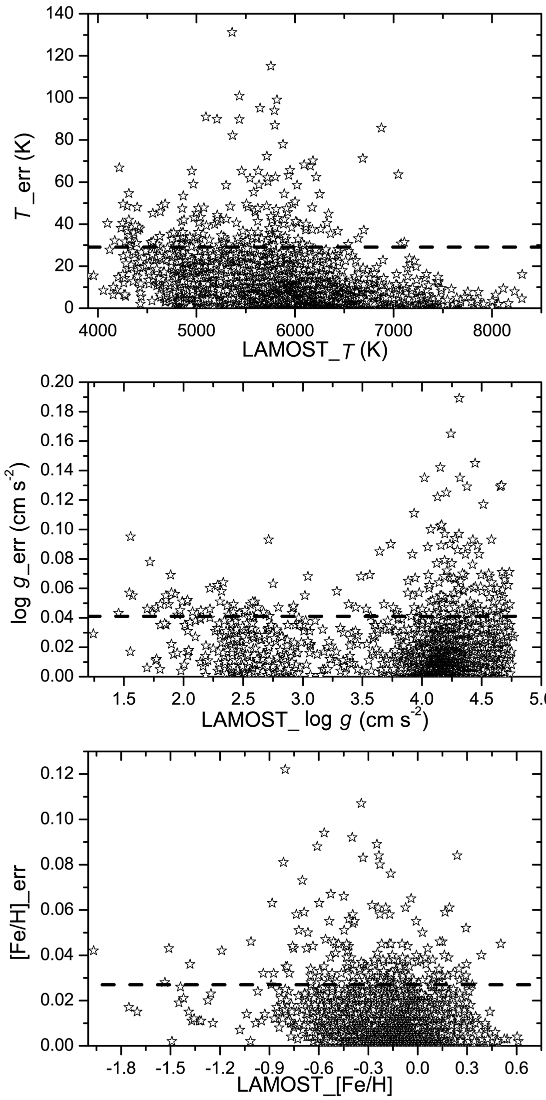

Fig. 2 Distributions of standard errors along with stellar atmospheric parameters. The standard errors are derived by atmospheric parameters of stars observed eight times or more. The *dashed lines* indicate that, for about 90% of stars, their standard errors are lower than 29 K for T, 0.041 for $\log g$ and 0.027 for [Fe/H].

The stellar atmospheric parameters of the first 390 SBVCs are shown in Table 1. Their radial velocity differences are larger than $115\,\mathrm{km\,s^{-1}}$. The designations are shown in the first column which are related to their right ascensions (RA) and declinations (Dec). The observational dates are listed in Column (2) including the beginning and end dates, while those in Column (3) are the number of observations for a given target. Those listed in Columns (4)–(9) are the stellar atmospheric parameters, T_{eff}, $\log(g)$ and [Fe/H], and their standard errors where "–9999" and "9999" mean that no errors were provided by the original LAMOST data. The lowest and highest radial velocities and their errors are shown in Columns (10)–(13). The differences between the lowest and highest radial velocities and their standard errors are displayed in the last two columns. The whole catalog of the detected SBVCs is available from the electronic version[6].

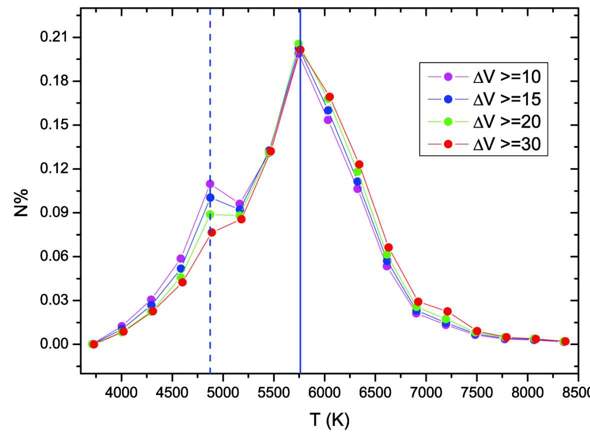

Fig. 3 The relative distribution of effective temperature for new SBVCs. *Colored solid dots* refer to targets with different radial velocity differences $\Delta V\ >10$, 15, 20 and $30\,\mathrm{km\,s^{-1}}$. The *solid* and *dashed blue lines* indicate the two peaks around 5760 K and 4870 K respectively.

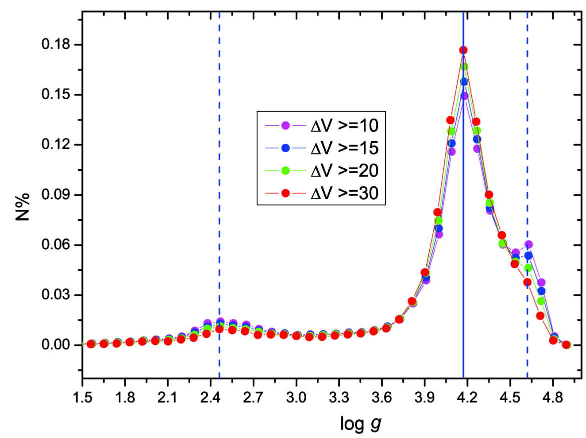

Fig. 4 The same as those in Fig. 3 but for the relative distributions of gravitational acceleration $\log(g)$. The *solid* and *dashed blue lines* refer to the three peaks around 2.461, 4.171 and $4.621\,\mathrm{cm\,s^{-2}}$, respectively.

3 DISTRIBUTIONS OF STELLAR ATMOSPHERIC PARAMETERS FOR NEW SBVCS

In this section, we analyze the distributions of effective temperature T_{eff}, gravitational acceleration $\log(g)$ and metallicity [Fe/H] for newly detected SBVCs. For comparison, in the following sections, we also investigate different

[6] *http://search.vbscn.com/variable_star.table1.txt*

Table 1 Stellar Atmospheric Parameters for SBVCs Detected by LAMOST (*http://search.vbscn.com/variable_star.table1.txt*)

Designation	Date-range	N	T (K)	Error	$\log(g)$	Error	[Fe/H]	Error	$V_{\rm r-low}$	Error	$V_{\rm r-high}$	Error	$\Delta V_{\rm r}$	Error
(1)	(2)	(3)	(4)	(5)	(6)	(7)	(8)	(9)	(10)	(11)	(12)	(13)	(14)	(15)
C060909.69+211524.7	2013-10-17–2017-03-16	5	4746.35	21.93	2.397	0.030	–0.196	0.021	7.90	9.26	416.84	8.29	408.94	12.43
C080100.51-025441.4	2012-12-22–2013-01-28	2	5986.35	124.45	4.119	0.179	–1.190	0.116	–5.55	12.32	401.73	13.19	407.28	18.05
C193009.84+390742.0	2012-06-15–2017-06-13	3	6083.49	9.06	4.364	0.011	0.197	0.009	–77.20	4.77	326.16	–9999.00	403.36	9999.00
C005615.70+392651.9	2013-11-25–2015-09-13	2	6441.47	151.58	4.300	0.218	–0.151	0.141	–376.81	12.75	20.92	23.30	397.73	26.56
C060841.96+221819.5	2016-12-01–2017-03-27	10	6473.63	2.51	4.203	0.002	–0.336	0.002	–32.47	14.16	359.78	1.96	392.25	14.30
C060331.31+230716.9	2016-12-01–2016-12-26	4	5071.10	51.88	2.481	0.074	–0.260	0.048	46.86	15.43	431.32	5.75	384.46	16.47
C113555.56+040439.0	2016-01-07–2017-03-08	2	5010.37	101.49	2.534	0.145	–0.962	0.095	–14.40	13.33	357.03	9.54	371.43	16.39
C060600.60+231514.1	2016-12-01–2017-03-27	12	4740.35	35.29	2.560	0.049	–0.097	0.033	–325.56	21.84	37.28	22.13	362.84	31.09
C060708.75+231912.9	2016-01-03–2017-03-27	12	5013.12	4.92	4.669	0.003	0.064	0.004	–332.18	7.45	1.21	3.86	333.39	8.39
C060920.95+221819.5	2016-12-01–2017-03-27	7	4920.90	47.76	2.234	0.068	–0.457	0.045	21.07	9.58	325.64	13.77	304.57	16.77
C191117.64+435907.2	2013-05-19–2015-10-11	2	4383.33	15.00	1.026	0.020	–1.430	0.014	–319.35	1.81	–17.92	22.03	301.43	22.10
C060707.17+232557.1	2016-12-01–2017-03-27	11	5726.68	15.27	4.470	0.020	–0.001	0.014	–312.08	8.53	–19.11	2.82	292.97	8.98
C062107.36+231416.2	2016-01-03–2016-12-26	5	4879.99	9.06	4.715	0.010	–0.006	0.009	–269.68	9.00	16.98	2.89	286.66	9.45
C103708.61+264412.6	2014-11-21–2017-01-24	3	5873.88	19.99	4.145	0.027	0.193	0.019	–38.53	2.53	243.08	19.78	281.61	19.94
C061245.53+205631.2	2016-01-03–2017-03-27	12	5984.66	2.60	4.040	0.002	–0.071	0.002	–9.99	2.23	260.32	2.79	270.31	3.57
C060909.90+220240.9	2016-12-01–2017-03-27	12	5737.46	9.96	4.352	0.013	0.158	0.009	33.42	5.93	302.67	8.85	269.25	10.65
C143624.77+564552.9	2017-05-01–2017-06-04	2	5817.87	4.75	4.594	0.003	0.071	0.004	–272.81	13.30	–5.07	1.04	267.74	13.34
C135246.97+161153.5	2015-04-13–2016-04-04	2	5776.12	348.73	4.230	0.501	–0.811	0.324	–86.26	25.49	181.19	–9999.00	267.45	9999.03
C113545.79+040225.1	2014-03-26–2016-01-19	4	5758.92	3.76	4.361	0.002	0.007	0.003	–13.02	17.46	251.25	10.44	264.27	20.34
C140813.24+074702.9	2015-02-07–2017-02-02	2	4756.56	118.59	2.121	0.170	–0.996	0.110	–124.43	15.17	136.83	10.81	261.26	18.63
C061320.95+204725.1	2013-10-17–2017-03-27	12	5430.70	9.51	4.653	0.012	0.124	0.009	31.54	22.01	286.81	14.32	255.27	26.26
C045242.82+122006.9	2013-11-24–2016-01-30	2	4022.55	78.30	4.211	0.111	–0.324	0.073	–65.65	10.48	188.66	8.13	254.31	13.26
C060542.69+232615.3	2013-11-12–2017-03-27	12	5397.23	7.75	4.460	0.009	–0.337	0.008	–271.04	5.97	-20.15	6.41	250.89	8.76
C012352.68-025010.7	2013-10-29–2014-01-09	4	4696.93	53.06	4.390	0.075	–0.293	0.050	–103.56	13.06	143.70	12.14	247.26	17.83
C060912.46+221554.0	2016-12-01–2017-03-27	12	6162.46	8.62	4.055	0.011	–0.356	0.008	1.25	3.90	242.75	2.37	241.50	4.56
C061203.91+205321.3	2016-12-01–2017-01-06	5	6494.58	6.93	4.082	0.009	–0.428	0.007	–55.21	14.05	180.51	2.16	235.72	14.22
C095647.37+562529.8	2013-04-18–2017-03-09	3	5794.78	9.68	4.069	0.012	–0.708	0.009	–213.64	17.71	20.34	1.28	233.98	17.76
C025338.80+001718.5	2015-10-08–2016-11-23	2	5216.47	28.51	2.453	0.040	–1.006	0.027	–35.02	14.98	196.31	2.92	231.33	15.26
C090635.08+314022.2	2012-02-02–2013-12-23	3	5882.42	97.45	4.069	0.139	–0.699	0.091	–37.47	31.13	189.32	8.47	226.79	32.26
C062848.07+404635.6	2015-02-12–2015-02-23	2	5710.43	211.18	3.543	0.303	–1.161	0.196	–229.73	18.87	–4.32	28.60	225.41	34.26
C015146.67+291715.8	2012-01-04–2012-01-13	2	5883.16	196.28	4.117	0.282	–0.730	0.182	–350.49	25.99	–128.12	17.11	222.37	31.12
C060638.44+232545.1	2016-12-01–2017-03-27	11	5023.80	40.70	2.319	0.058	–0.263	0.038	–161.48	10.82	59.31	19.83	220.79	22.59
C061845.99+232419.9	2016-02-20–2017-03-27	11	5259.22	6.90	4.376	0.007	–0.076	0.006	–172.23	6.31	47.01	8.59	219.24	10.66
C072504.02-005523.2	2012-12-03–2016-03-07	2	7118.82	38.64	4.124	0.054	–0.448	0.036	–40.57	12.42	174.63	3.58	215.20	12.93
C060618.91+231519.4	2016-01-03–2017-03-27	13	4975.37	17.48	2.350	0.023	–0.575	0.017	–222.64	6.33	–9.87	14.41	212.77	15.74
C093212.66+281731.3	2012-02-09–2017-03-17	2	5563.51	90.32	3.611	0.129	–1.460	0.084	–32.08	42.78	180.44	7.42	212.52	43.42
C223819.22+173733.2	2013-10-14–2016-11-12	2	5196.73	48.28	4.333	0.069	–0.027	0.045	–118.98	4.57	92.31	7.91	211.29	9.14
C071343.46+223555.5	2013-11-14–2013-11-24	4	6675.60	5.05	4.194	0.006	–0.302	0.005	–90.08	0.98	119.29	2.38	209.37	2.57
C060524.16+244923.4	2016-12-01–2017-03-27	11	6681.84	8.36	4.023	0.011	–0.409	0.008	–40.69	12.57	167.12	1.78	207.81	12.70
C061257.59+204945.7	2016-12-01–2017-03-27	9	5739.94	27.30	4.514	0.039	–0.152	0.026	–15.76	4.80	188.56	6.11	204.32	7.77
C154538.03+531828.3	2012-06-17–2016-02-19	3	5166.81	72.10	4.344	0.102	–0.041	0.067	–144.63	13.41	56.06	24.13	200.69	27.61
C072142.66+474246.5	2016-03-11–2016-03-13	2	4382.88	119.43	4.543	0.170	–0.396	0.111	–270.58	21.08	–72.28	10.38	198.30	23.50
C060641.86+231958.5	2013-10-17–2017-03-27	13	5767.42	2.54	4.341	0.002	–0.429	0.002	–168.01	2.36	29.55	1.03	197.56	2.57
C110035.82+274749.8	2011-12-11–2013-12-11	3	5050.58	124.75	2.583	0.179	–0.914	0.116	–171.23	16.93	25.10	18.19	196.33	24.85
C012129.49+381544.1	2013-12-13–2015-12-21	2	4969.34	116.91	2.273	0.167	–1.762	0.109	–276.29	10.64	–81.42	15.55	194.87	18.84
C125556.57+565846.4	2013-05-12–2016-03-27	2	6220.09	4.51	4.102	0.005	–0.487	0.005	–108.10	1.70	84.82	0.88	192.92	1.91
C080637.38+240242.5	2013-01-07–2016-01-31	4	6126.81	135.38	4.104	0.193	–1.419	0.126	–21.86	37.83	170.91	14.17	192.77	40.40
C011210.47+365628.2	2014-12-22–2015-10-29	2	6104.16	149.47	4.103	0.214	–1.447	0.139	–357.98	16.10	–168.00	16.07	189.98	22.75
C060336.34+240938.1	2016-12-01–2016-12-02	2	6946.52	145.75	3.915	0.209	0.011	0.135	16.32	15.81	205.06	15.10	188.74	21.86
C105242.73+182923.9	2014-12-21–2017-04-23	2	5899.64	185.96	3.733	0.267	–0.641	0.173	91.09	21.26	279.22	17.30	188.13	27.41
C060828.00+232827.5	2016-12-01–2017-01-06	5	4956.62	8.89	2.483	0.008	–0.415	0.008	–168.67	6.47	18.77	2.54	187.44	6.95
C033742.62+404711.2	2015-01-12–2016-01-10	3	6654.46	28.60	4.146	0.040	–0.316	0.027	–120.44	3.09	66.89	9.66	187.33	10.14
C110139.95+314619.4	2012-01-05–2015-01-10	4	5758.56	14.08	4.349	0.019	0.028	0.013	–69.92	2.42	116.29	2.55	186.21	3.52
C060322.46+232530.7	2014-01-10–2017-02-26	8	4704.64	28.55	2.221	0.040	–0.206	0.027	–135.74	13.42	50.07	7.75	185.81	15.50
C060234.17+225318.6	2013-10-17–2017-03-27	13	6440.52	2.57	4.104	0.003	–0.007	0.002	13.31	5.24	197.93	1.72	184.62	5.52
C061628.33+232933.1	2016-01-19–2017-03-27	13	7193.28	0.65	4.087	0.000	–0.136	0.001	–85.75	0.39	98.13	1.34	183.88	1.40
C195457.87+395421.4	2013-10-05–2015-10-08	3	4506.26	81.01	2.208	0.117	–0.133	0.075	–79.64	10.59	104.06	13.26	183.70	16.97
C041944.32+442808.3	2013-12-13–2014-12-01	3	5921.63	41.50	4.182	0.058	–0.262	0.039	–123.61	4.35	59.89	16.52	183.50	17.08
C061346.08+221846.9	2013-10-17–2016-12-02	4	5785.50	61.92	1.309	0.088	–0.084	0.058	–166.90	17.32	14.93	11.88	181.83	21.00

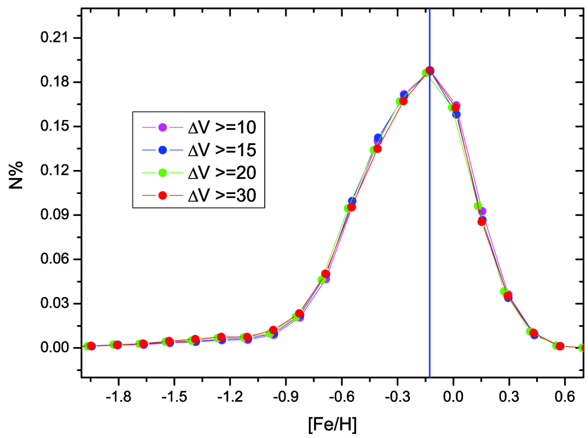

Fig. 5 The same as those in Figs. 3 and 4 but for the distributions of metallicity [Fe/H]. The *solid blue line* represents the main peak around –0.128 dex.

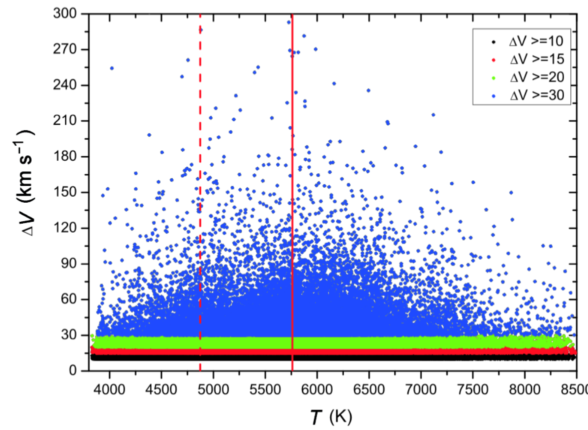

Fig. 6 The distribution of radial velocity along with effective temperature. *Colored dots* represent SBVCs with different criterions ΔV >10, 15, 20 and 30 km s^{-1}. The *solid* and *dashed red lines* refer to the two peaks in the temperature distribution.

sets of targets by considering different criterions ΔV >15, 20 and 30 km s^{-1}. The distribution of the effective temperature is shown in Figure 3 where colored solid dots represent SBVCs with different radial velocity differences ΔV >10, 15, 20 and 30 km s^{-1}. As shown in the figure, there are two peaks for the temperature distribution. The main peak is around 5760 K which is close to the temperature of the Sun. The other peak is near 4870 K indicating that some SBVCs are cool stars. Since most of the stars in the Universe are red dwarfs, this peak may correspond to red dwarf binaries or some evolved cool pulsating stars.

The distributions of gravitational acceleration $\log(g)$ for SBVCs are displayed in Figure 4. Three peaks are visible in the distributions. The first peak is around 4.171 cm s^{-2}, while the other two peaks are near 2.461 and 4.621 cm s^{-2}. The three peaks indicate that there are several groups of SBVCs. Their structure and evolutionary states are quite different and will be discussed later. The metallicity ([Fe/H]) distribution is shown in Figure 5 where the peak is around –0.128. This indicates that the metallicities of most SBVCs are slightly lower than that of the Sun. The metal peak is close to the peak for EA-type binaries (–0.148) reported by Qian et al. (2018b). The distributions of radial velocity along with effective temperature, gravitational acceleration $\log(g)$ and metallicity [Fe/H] are depicted in Figures 6–8. Like those in Figures 3–5, the colored dots in those figures represent SBVCs with different criterions ΔV >10, 15, 20 and 30 km s^{-1}. The peaks of the distributions for the stellar parameters are also shown as solid and dashed red lines.

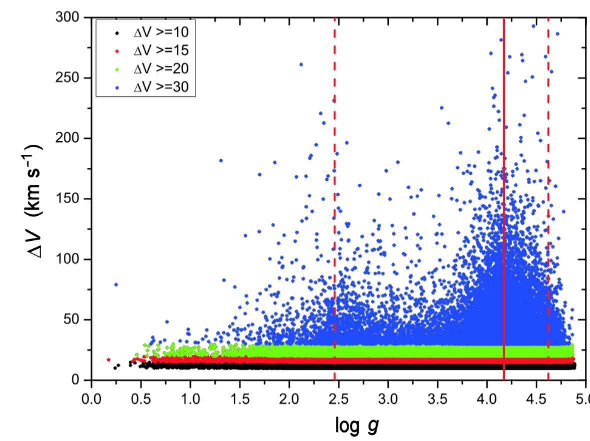

Fig. 7 The same as those in Fig. 6 but for the distribution of radial velocity along with gravitational acceleration $\log(g)$. The *solid* and *dashed red lines* refer to the three peaks in the relative distributions for gravitational acceleration.

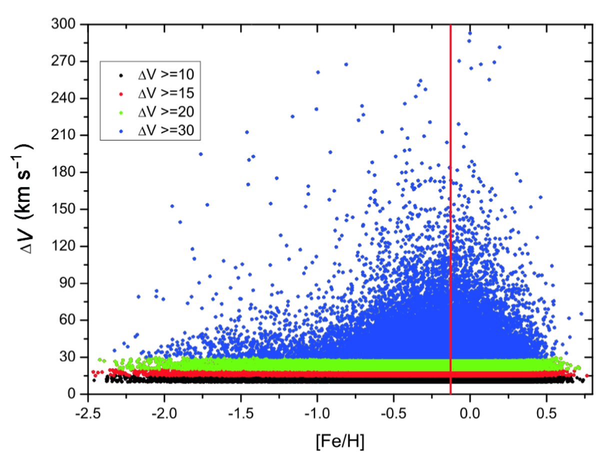

Fig. 8 The same as those in Figs. 6 and 7 but for the distribution of radial velocity along with metallicity [Fe/H]. The *solid red line* represents the main peak in the distribution of metallicity.

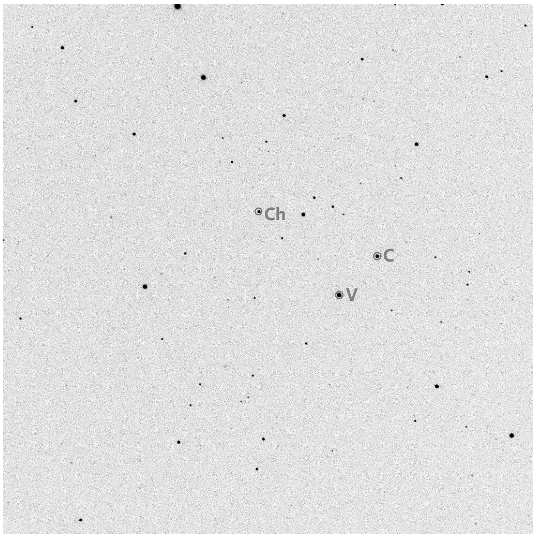

Fig. 9 A CCD image of the field of view around C1346. "V" represents the variable star C1346, while "C" refers to the comparison star and "Ch" to the check star.

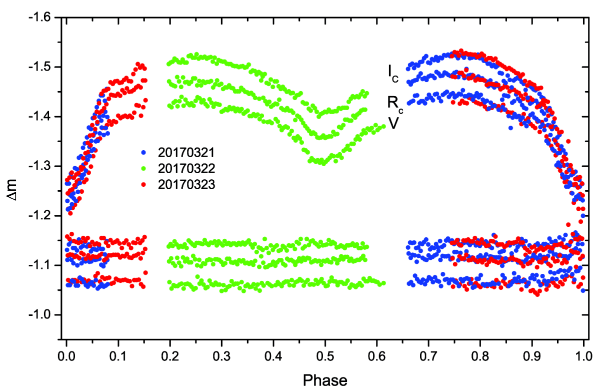

Fig. 10 CCD photometric light curves of C1346 obtained by using the 70-cm Sino-Thai telescope in Lijiang. The magnitude differences between the comparison and check stars are also shown. *Solid dots with different colors* refer to data obtained in different nights.

4 DETECTION OF A NEW ECLIPSING BINARY C134624+333921.2

During the time interval from January 2013 to January 2017, C134624.29+333921.2 (hereafter C1346) was observed by LAMOST three times. The difference between the lowest and highest radial velocities is about $165\,\mathrm{km\,s^{-1}}$. The large radial velocity difference indicates that it is an SBVC and is most probably a binary candidate. The mean temperature $T = 6009.15(\pm 4.90)\,\mathrm{K}$ and gravitational acceleration $\log(g) = 4.201(\pm 0.005)\,\mathrm{cm\,s^{-2}}$ suggest that it slightly evolved from the zero-age main sequence (ZAMS) stage (Cox 2000). Its metallicity of [Fe/H]= $0.016(\pm 0.005)$ dex is close to that of the Sun.

Table 2 Photometric solutions of C1346

Parameter	Value
g_1	0.32 (fixed)
g_2	0.32 (fixed)
A_1	0.50 (fixed)
A_2	0.50 (fixed)
q (M_2/M_1)	0.46($\pm$0.02)
T_1 (K)	6016 (fixed)
i ($^\circ$)	75.3($\pm$0.8)
$\Omega_{\rm in}$	2.78
$\Omega_{\rm out}$	2.51
Ω_1	3.10($\pm$0.03)
Ω_2	4.33($\pm$0.19)
T_2 (K)	4615($\pm$27)
ΔT (K)	1401
T_2/T_1	0.767($\pm$0.004)
$L_1/(L_1+L_2)\,(V)$	0.9666($\pm$0.0001)
$L_1/(L_1+L_2)\,(R_c)$	0.9569($\pm$0.0002)
$L_1/(L_1+L_2)\,(I_c)$	0.9488($\pm$0.0002)
r_1 (pole)	0.376($\pm$0.003)
r_1 (point)	0.424($\pm$0.003)
r_1 (side)	0.392($\pm$0.003)
r_1 (back)	0.407($\pm$0.003)
r_2 (pole)	0.151($\pm$0.011)
r_2 (point)	0.154($\pm$0.012)
r_2 (side)	0.152($\pm$0.011)
r_2 (back)	0.154($\pm$0.012)
θ ($^\circ$)	69.1($\pm$14.9)
ψ ($^\circ$)	3.9($\pm$6.7)
r (rad)	0.42($\pm$0.06)
T_f	0.87(fixed)
$\Sigma\omega(O-C)^2$	0.01787

To confirm whether it is a variable star or not, it was observed using the 70-cm Sino-Thai telescope on 2017 March 21–23. The telescope is located at Lijiang Observing Station, which is administered by Yunnan Observatories in China. During the observing process, an Andor 2048×2048 CCD photometric system together with the $V(RI)_c$ filters was used. A finding chart including C1346, the comparison star and the check star is displayed in Figure 9. The observed CCD images were reduced by using PHOT of the IRAF aperture photometry package. The phased three-color light curves computed by applying the linear ephemeris, Min. I= 2457834.39005 + $0.65^{\rm d} \times E$, are plotted in Figure 10. The differential magnitudes between the comparison (C) and check (Ch) stars are also plotted in the lower part of the figure. As shown in Figure 10, the light curves are EB-type and exhibit the O'Connell effect where the maxima following the primary minima are slightly lower than the other ones.

The $V(RI)_c$ light curves were simultaneously analyzed with the 2013 version of the Wilson+Devinney (W-D) program (Wilson & Devinney 1971; Wilson 1979,

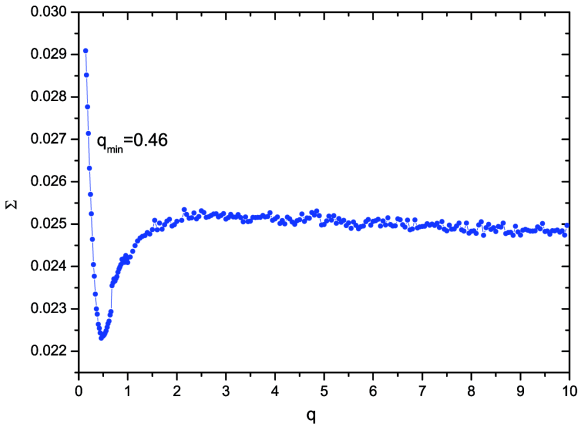

Fig. 11 The relation between Σ and q for C1346.

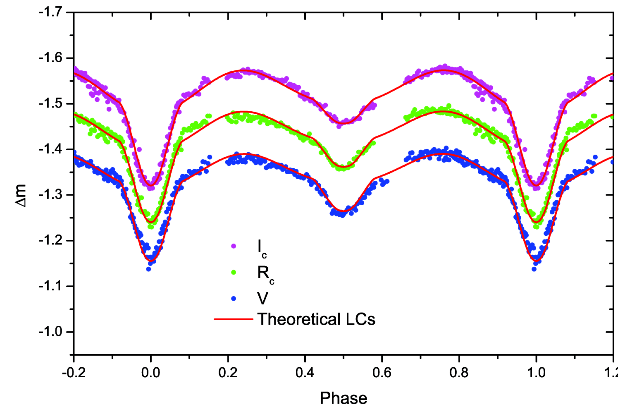

Fig. 12 Observed (*colored solid dots*) and theoretical (*red lines*) light curves in VRI bands for C1346.

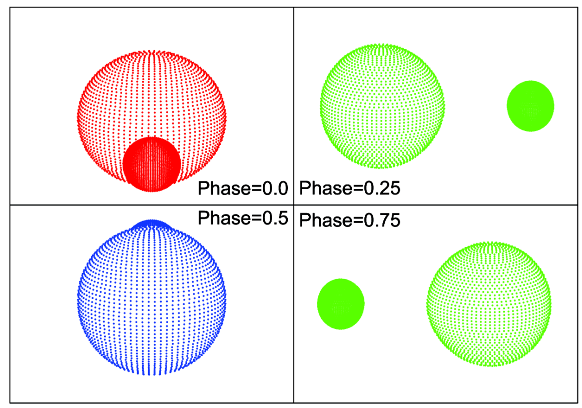

Fig. 13 Geometrical structure of the detached binary system C1346 at phases 0.0, 0.25, 0.50 and 0.75.

1990). The effective temperature of Star 1 (the star eclipsed at the primary minimum) was fixed at the LAMOST values, i.e., $T_1 = 6009.15\,\mathrm{K}$. The gravity-darkening coefficients $g_{1,2} = 0.32$ and the bolometric albedos $A_{1,2} = 0.5$ were applied because both components are cool stars (e.g., Lucy 1967; Ruciński 1969). An internal calculation with the logarithmic law was used to determine the bolometric and bandpass limb-darkening coefficients (e.g., van Hamme 1993).

A q-search method was used to obtain initial values of those parameters including the mass ratio q, orbital inclination i, mean temperature of Star 2 T_2, monochromatic luminosity of Star 1 L_1, and dimensionless potentials Ω_1 and Ω_2 for Star 1 and Star 2 respectively. During the q-search process, a series of trial values for q were assumed. The resulting sum of squared residuals Σ for each q is plotted in Figure 11 where a minimum value of Σ is achieved at $q = 0.46$. The final photometric solutions for C1346 were obtained and are listed in Table 2 by performing a series of differential corrections. Theoretical light curves (red line) computed with those solutions are shown in Figure 12. Our solutions reveal that C1346 is a detached binary in which the primary is filling its critical Roche lobe by about 89%. The geometrical structures of the detached binary system at phases 0.0, 0.25, 0.50 and 0.75 are displayed in Figure 13. The secondary is a cool star with a temperature of 4615 K. The asymmetries of the light curves are explained as a dark spot on this component.

5 SEVERAL STATISTICAL CORRELATIONS FOR NEW SBVCS

The correlations between metallicity and effective temperature for those SBVCs are shown in Figure 14. Solid dots with different colors represent those targets with different radial velocity differences $\Delta V >$10, 15, 20 and 30 km s^{-1}. It is apparent that their distributions are the same. The solid and dashed red lines in the figure refer to the peaks of the temperature distribution. As shown in the figure, the metallicity of hotter SBVCs with $T > 6300\,\mathrm{K}$ is usually higher than –1.0. The lower limit of metallicity is correlated with temperature and it is increasing along with temperature. Some investigations have demonstrated that stellar metallicities are weakly correlated with their ages for stars in the Galaxy (e.g., Reid et al. 2007; Feltzing & Bensby 2009), and higher metallicities of hotter SBVCs may indicate that they are usually young and newly formed objects. The metallicities of some hotter SBVCs are higher than 0.5, suggesting that they are extremely young objects or they may be contaminated by material from the evolution of unseen neutron star or black hole companions as mentioned by Qian et al. (2017, 2018b). The metallicity distribution of cooler SBVCs with $T < 6300\,\mathrm{K}$ is usually in a large range from –2.5 to 0.5 dex.

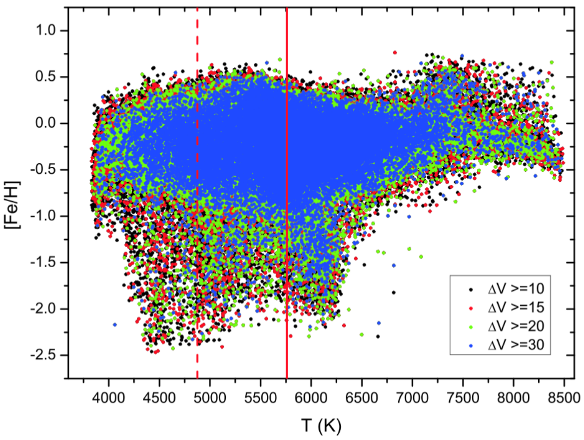

Fig. 14 The correlations between the metallicity and effective temperature for those new SBVCs. *Solid dots with different colors* refer to targets with different criterions ΔV >10, 15, 20 and 30 km s^{-1}. The *solid* and *dashed red lines* represent to the peaks of the temperature distribution.

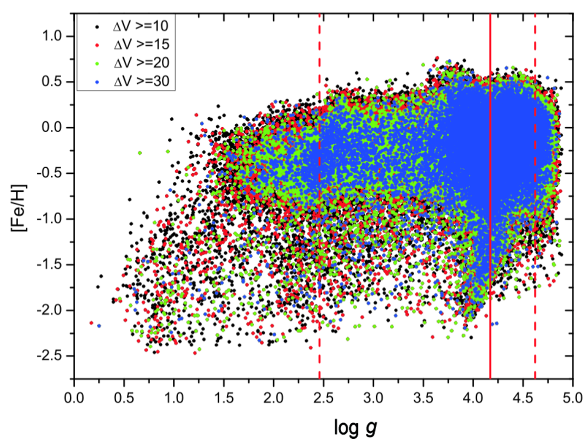

Fig. 15 The same as those in Fig. 14 but for the correlations between metallicity and gravitational acceleration. The *solid* and *dashed red lines* refer to peaks of the $\log(g)$ distributions.

The relations between metallicity and gravitational acceleration are shown in Figure 15. The solid red line represents the main peak of the distribution of gravitational acceleration, while the two dashed lines refer to the other two smaller peaks. As displayed in the figure, metallicity is weakly correlated with gravitational acceleration. Both the low and high limits of metallicity increase along with the increase in gravitational acceleration. This could be explained by the fact that evolved targets (with lower gravitational acceleration) are older than main sequence stars and have lower metallicity. There is a group of SBVCs with metallicities lower than –1.0 and gravitational accelerations lower than 3.8. They have evolved from the main sequence and include subgiants, giants and supergiants. The variations of radial velocities are mainly caused by pulsation. They are good objects for studying stellar structures and evolutions at late stages.

The relations between $\log(g)$ and T are displayed in Figure 16. Those plotted in the top-left panel of the figure are for all SBVCs found by LAMOST. For comparison, the targets with radial velocities larger than 15, 20 and 30 km s^{-1} are also shown in the other three panels. It is apparent that they have the same distribution. The solid magenta line at the bottom of each panel stands for ZAMS that is from Cox (2000), while the other magenta lines represent the luminosity classes ranging from Ia to V that are from Straizys & Kuriliene (1981). As displayed in the figure, most of the SBVCs are main sequence stars or slightly evolved from the main sequence (e.g., subgiants) with temperatures in the range from 3800 K to 8500 K. Most of them may be binary stars or pulsating variables including δ Sct and γ Dor stars. It is interesting to point out that some of the SBVCs are giants or supergiants. To understand their physical properties, more photometric and spectroscopic data are required in the future.

Among the 256 thousand SBVCs detected by LAMOST, 19 862 of them were also observed by *Gaia* (Gaia Collaboration et al. 2016b). The apparent magnitudes and parallaxes were given in *Gaia* Data Release 1 (Gaia Collaboration, Gaia Collaboration et al. 2016a). By using LAMOST and *Gaia* data, the Hertzsprung-Russell (H-R) diagram for those SBVCs was constructed and is plotted in Figure 17 where the effective temperature is from LAMOST. The ZAMS from Kippenhahn et al. (2012) is plotted as the solid magenta line at the bottom. Also shown as solid magenta lines in the figure are the luminosity classes ranging from Ia to V that are from Straizys & Kuriliene (1981). Like those displayed in other figures, different symbols refer to binary and variable candidates with different radial velocity differences ΔV >10, 15, 20 and 30 km s^{-1}. The shape of the distribution is the same as those shown in Figure 16. It is more clearly seen that most of the targets are main sequence stars or subgiants and some of them are giants or supergiants. It is detected that a group of SBVCs is below ZAMS. They may be interesting targets at a special stellar evolutionary stage and we will focus on them in future work.

6 DISCUSSION AND CONCLUSIONS

During the first stage of the LAMOST spectroscopic survey, about 786.4 thousand stars were observed twice or more from 2011 October 24 to 2017 July 16. After removing known variable stars, we found that there are about 256 thousand stars with radial velocity differences ($\Delta V_{\rm r}$ larger

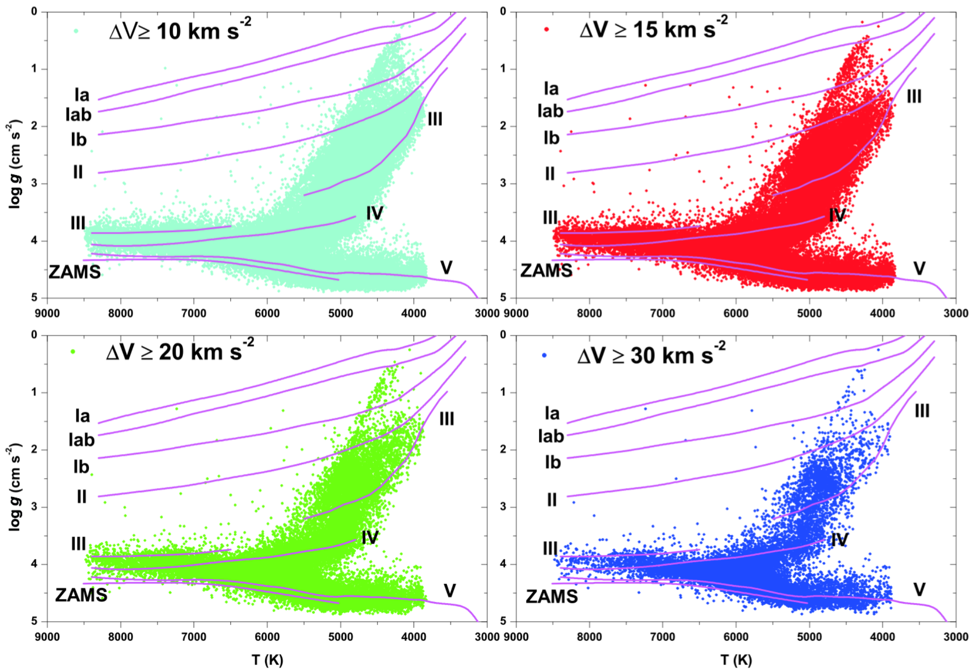

Fig. 16 The correlations between gravitational acceleration and effective temperature. The *magenta lines* in the four panels stand for the luminosity classes, ranging between Ia and V, which are from Straizys & Kuriliene (1981), while the ZAMS line is from Cox (2000).

than $10\,\mathrm{km\,s^{-1}}$) and they are possibly SBVCs. Their stellar atmospheric parameters are cataloged and we present those of the first 390 SBVCs in Table 1 with radial velocity differences larger than $115\,\mathrm{km\,s^{-1}}$. There are about 4575 variables listed in VSX which were also observed by LAMOST two times or more. To understand what types of SBVCs they could be, we construct the number distributions for VSX variable stars along with their types. It is plotted in Figure 18 in the order of decreasing number where the types of those variables are from the variability classification of the General Catalogue of Variable Stars (GCVS) scheme[7] (e.g., Watson et al. 2006; Samus' et al. 2017). As shown in the figure, the first and second large number of targets are EW- and EA-type EBs and then are pulsating stars including RR Lyrae and δ Scuti variables. This indicates that most of SBVCs may be binary systems, which could be explained by the fact that most of the stars in the Galaxy are in binaries (including multiple systems).

C1346 is one of the SBVCs with a radial velocity difference of about $165\,\mathrm{km\,s^{-1}}$ and most probably it is a binary candidate. To confirm this conclusion, it was observed by using the Sino-Thai 70-cm telescope in March 2017. It is found that C1346 is an EB with a period of 0.65 days. A preliminary investigation with the W-D method suggests that it is a detached binary system with a mass ratio of 0.46. The primary is filling its critical Roche lobe by about 89%, while the secondary is only filling 48% of it. The mean temperature $T = 6009.15(\pm4.90)\,\mathrm{K}$ and the metallicity [Fe/H]$=0.016(\pm0.005)$ dex indicate that the primary component is a solar-type star, while the gravitational acceleration $\log(g) = 4.201(\pm0.005)\,\mathrm{cm\,s^{-2}}$ reveals that it slightly evolved from the ZAMS stage (Cox 2000). These properties suggest that the primary will evolve to fill its critical Roche lobe and mass transfer will occur between the two components. The temperature of the secondary is about 4615 K, indicating that it is a cool red dwarf star. The asymmetries of the light curves can be explained as dark spot activity on this cool component.

In Section 3, the distributions of temperature (T), gravitational acceleration ($\log g$) and metallicity [Fe/H] for those SBVCs are presented and analyzed. It is shown that the peak of the metallicity distribution is at -0.128 indicating that most SBVCs are slightly metal poorer than the Sun. There are two peaks in the temperature distribution around 5760 K and 4870 K, while there are three peaks in the distribution of gravitational acceleration ($\log g$) at 2.461, 4.171 and $4.621\,\mathrm{cm\,s^{-2}}$. The distribution peak for gravitational acceleration around $4.621\,\mathrm{cm\,s^{-2}}$ may correspond to the temperature peak at 4870 K, indicating that some of the SBVCs are red dwarf binary stars. This is in agreement with the fact that a large number of stars in the Universe are red dwarfs.

[7] `http://www.aavso.org/vsx/index.php?view=about.vartypes`

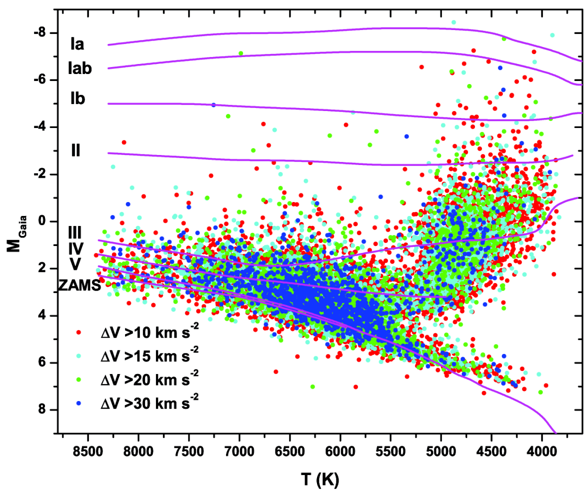

Fig. 17 The H-R diagram for those SBVCs observed by both LAMOST and *Gaia*. The *magenta lines* refer to the luminosity classes that range between Ia and V and ZAMS.

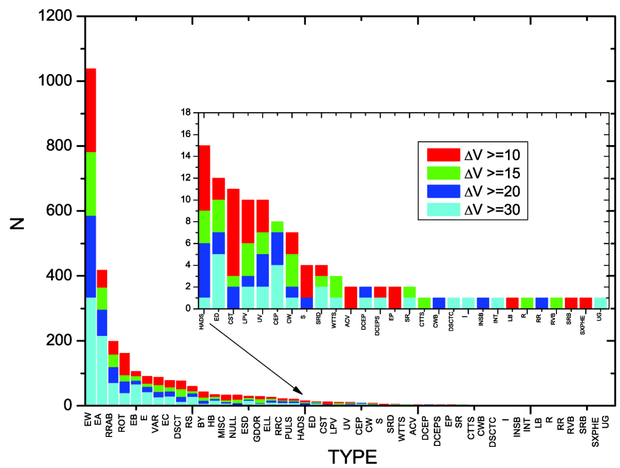

Fig. 18 Distributions of VSX variable stars along with the types. All of them were observed by LAMOST twice or more. Different colors represent different criterions with $\Delta V > 10$, 15, 20 and 30 km s^{-1}.

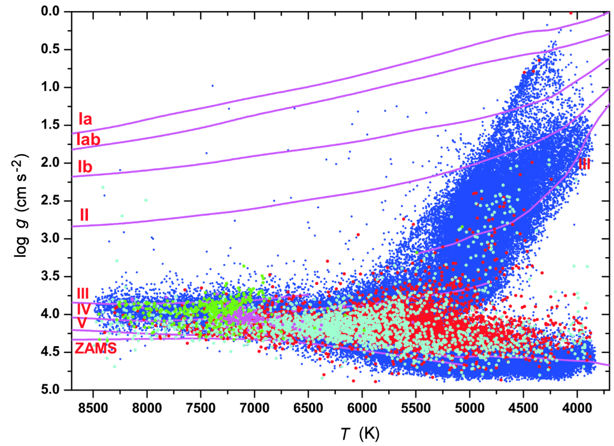

Fig. 19 Comparisons between different types of pulsating stars and binaries with SBVCs in the $\log(g)$-T diagram. The magenta lines are the same as those in Fig. 17. *Green* and *magenta dots* refer to normal δ Scuti and γ Dor variables respectively, while *cyan* and *red dots* to EA- and EW-type binary stars respectively.

Many δ Sct and γ Dor stars (Qian et al. 2018a, 2019), and binary systems including EW- and EA-type binaries (Qian et al. 2017, 2018b), were observed by LAMOST and their stellar parameters are presented and investigated. The locations of SBVCs on the $\log g$-T diagram are compared with those of known variables analyzed by Qian et al. (2017, 2018a,b, 2019) and are shown in Figure 19. As displayed in the figure, the main peak of the gravitational acceleration around 4.171 cm s^{-2} is caused by the distributions of EW- and EA-type binaries together with pulsating stars that are at the low-luminosity part of the Cepheid instability strip in the H-R diagram. These properties reveal that most of the SBVCs may be binary systems or pulsating stars at the low-luminosity part of the Cepheid instability strip, such as δ Sct and γ Dor variables. As displayed in Figures 16, 17 and 19, there is a group of SBVCs that has higher gravitational accelerations and some of them are below the ZAMS. They may be contact binaries (e.g., W UMa-type binary stars) where both components are sharing a common envelope. The primaries are losing energy to the secondaries in the common envelopes and are at a special stellar evolutionary stage.

The correlation between metallicity and effective temperature for SBVCs is plotted in Figure 14. It is shown that the metallicity of hotter SBVCs with $T > 6300$ K is correlated with the temperature, while the metallicity distribution of cooler SBVCs with $T < 6300$ K has a large range from –2.5 to 0.5 dex. The higher metallicity of hotter SBVCs is along with the higher temperature. This may indicate that they are usually young and are newly formed objects. Some hotter SBVCs with extremely higher metallicities ([Fe/H]$>$ 0.5 dex) may be contaminated by material from the evolution of unseen neutron star or black hole companions as mentioned by Qian et al. (2017, 2018b). The correlation between metallicity and gravitational acceleration shown in Figure 15 reveals that the metallicity is weakly correlated with gravitational acceleration. The metallicity increases along with the increase of gravitational acceleration. This reveals that evolved targets (that have lower gravitational acceleration) are older than main sequence stars and have lower metallicity. As we can see in both of the two figures, there is an evolved group of SBVCs with gravitational accelerations lower than 3.8 cm s^{-2}. Their metallicities are lower than –1.0 dex and temperatures are below 5800 K. The small peak in the distribution of gravitational acceleration around 2.461 cm s^{-2} is mainly caused by the presence of the group of SBVCs. They have evolved from the main sequence and may be pulsating giants and supergiants. This group of old stars represents good targets to investigate stellar structures and evolutions at late evolutionary stages.

Acknowledgements The Guo Shou Jing Telescope (the Large Sky Area Multi-Object Fiber Spectroscopic Telescope, LAMOST) is a National Major Scientific Project built by the Chinese Academy of Sciences. Funding for the project has been provided by the National Development and Reform Commission. LAMOST is operated and managed by National Astronomical Observatories, Chinese Academy of Sciences. Spectroscopic observations of those stars used in the paper were obtained with LAMOST from 2011 October 24 to 2017 July 16. New CCD photometric observations of C1346 were acquired with the 70-cm Sino-Thai telescope at Lijiang Observing Station administered by Yunnan Observatories in China.

References

Andersen, J. 1991, A&A Rev., 3, 91
Bakos, G., Noyes, R. W., Kovács, G., et al. 2004, PASP, 116, 266
Borucki, W. J., Koch, D., Basri, G., et al. 2010, Science, 327, 977
Breger, M., Hutchins, J., & Kuhi, L. V. 1976, ApJ, 210, 163
Cox, A. N. 2000, Allen's Astrophysical Quantities, (4th edn.; New York: Springer)
Cui, X.-Q., Zhao, Y.-H., Chu, Y.-Q., et al. 2012, RAA (Research in Astronomy and Astrophysics), 12, 1197
De Cat, P., Eyer, L., Cuypers, J., et al. 2006, A&A, 449, 281
Drake, A. J., Djorgovski, S. G., Mahabal, A., et al. 2009, ApJ, 696, 870
Drake, A. J., Graham, M. J., Djorgovski, S. G., et al. 2014, ApJS, 213, 9
Feltzing, S., & Bensby, T. 2009, in IAU Symposium, 258, The Ages of Stars, eds. E. E. Mamajek, D. R. Soderblom, & R. F. G. Wyse, 23
Frasca, A., Alcalá, J. M., Covino, E., et al. 2003, A&A, 405, 149
Frasca, A., Guillout, P., Marilli, E., et al. 2006, A&A, 454, 301
Frasca, A., Molenda-Żakowicz, J., De Cat, P., et al. 2016, A&A, 594, A39
Gaia Collaboration, Brown, A. G. A., Vallenari, A., et al. 2016a, A&A, 595, A2
Gaia Collaboration, Prusti, T., de Bruijne, J. H. J., et al. 2016b, A&A, 595, A1
Gao, H., Zhang, H.-W., Xiang, M.-S., et al. 2015, RAA (Research in Astronomy and Astrophysics), 15, 2204
Hatzes, A. P. 1998, MNRAS, 299, 403
Howell, S. B., Sobeck, C., Haas, M., et al. 2014, PASP, 126, 398
Kippenhahn, R., Weigert, A., & Weiss, A. 2012, Stellar Structure and Evolution (Springer-Verlag Berlin Heidelberg)
Koleva, M., Prugniel, P., Bouchard, A., & Wu, Y. 2009, A&A, 501, 1269
Lucy, L. B. 1967, ZAp, 65, 89
Luo, A.-L., Zhao, Y.-H., Zhao, G., et al. 2015, RAA (Research in Astronomy and Astrophysics), 15, 1095
Mathias, P., Le Contel, J.-M., Chapellier, E., et al. 2004, A&A, 417, 189
Palaversa, L., Ivezić, Ž., Eyer, L., et al. 2013, AJ, 146, 101
Pepper, J., Kuhn, R. B., Siverd, R., James, D., & Stassun, K. 2012, PASP, 124, 230
Pojmanski, G. 1997, Acta Astronomica, 47, 467
Pojmanski, G., Pilecki, B., & Szczygiel, D. 2005, Acta Astronomica, 55, 275
Pollacco, D. L., Skillen, I., Collier Cameron, A., et al. 2006, PASP, 118, 1407
Qian, S.-B., He, J.-J., Zhang, J., et al. 2017, RAA (Research in Astronomy and Astrophysics), 17, 087
Qian, S.-B., Li, L.-J., He, J.-J., et al. 2018a, MNRAS, 475, 478
Qian, S.-B., Li, L.-J., He, J.-J., et al. 2019, RAA (Research in Astronomy and Astrophysics), 19, 1
Qian, S.-B., Zhang, J., He, J.-J., et al. 2018b, ApJS, 235, 5
Reid, I. N., Turner, E. L., Turnbull, M. C., Mountain, M., & Valenti, J. A. 2007, ApJ, 665, 767
Ruciński, S. M. 1969, Acta Astronomica, 19, 245
Samus', N. N., Kazarovets, E. V., Durlevich, O. V., Kireeva, N. N., & Pastukhova, E. N. 2017, Astronomy Reports, 61, 80
Straizys, V., & Kuriliene, G. 1981, Ap&SS, 80, 353
Torres, G., Andersen, J., & Giménez, A. 2010, A&A Rev., 18, 67
van Hamme, W. 1993, AJ, 106, 2096
Wang, S.-G., Su, D.-Q., Chu, Y.-Q., Cui, X., & Wang, Y.-N. 1996, Appl. Opt., 35, 5155
Watson, C. L., Henden, A. A., & Price, A. 2006, Society for Astronomical Sciences Annual Symposium, 25, 47
Wilson, R. E. 1979, ApJ, 234, 1054
Wilson, R. E. 1990, ApJ, 356, 613
Wilson, R. E., & Devinney, E. J. 1971, ApJ, 166, 605
Woźniak, P. R., Vestrand, W. T., Akerlof, C. W., et al. 2004, AJ, 127, 2436
Wu, Y., Luo, A.-L., Li, H.-N., et al. 2011, RAA (Research in Astronomy and Astrophysics), 11, 924
Wu, Y., Du, B., Luo, A., Zhao, Y., & Yuan, H. 2014, in IAU Symposium, 306, Statistical Challenges in 21st Century Cosmology, ed. A. Heavens, J.-L. Starck, & A. Krone-Martins, 340
Yang, S., & Walker, G. A. H. 1986, PASP, 98, 862
Zhao, G., Zhao, Y.-H., Chu, Y.-Q., Jing, Y.-P., & Deng, L.-C. 2012, RAA (Research in Astronomy and Astrophysics), 12, 723